Acta Crystallographica Section F
Structural Biology and Crystallization Communications
ISSN 1744-3091

Crystallization and X-ray diffraction analysis of the N-terminal domain of the Toll-like receptor signalling adaptor protein TRIF/TICAM-1

M. Obayed Ullah,[a,b] Thomas Ve,[a,b] Jameris Dkhar,[a,b] Mohammed Alaidarous,[a,b] Daniel J. Ericsson,[a,b] Matthew J. Sweet,[b,c] Ashley Mansell[d] and Bostjan Kobe[a,b,c]*

[a]School of Chemistry and Molecular Biosciences, University of Queensland, Brisbane, Queensland 4072, Australia, [b]Institute for Molecular Bioscience, University of Queensland, Brisbane, Queensland 4072, Australia, [c]Australian Infectious Diseases Research Centre, University of Queensland, Brisbane, Queensland 4072, Australia, and [d]Centre for Innate Immunity and Infectious Diseases, Monash Institute of Medical Research, Monash University, Melbourne, Victoria 3168, Australia

Correspondence e-mail: b.kobe@uq.edu.au

Received 16 April 2013
Accepted 22 May 2013

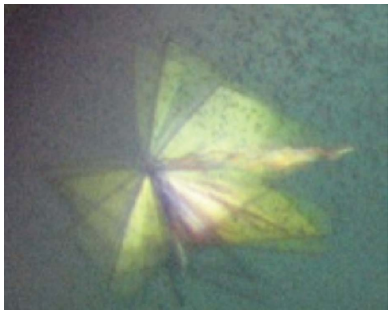

As part of the mammalian innate immune response, Toll-like receptors 3 and 4 can signal *via* the adaptor protein TRIF/TICAM-1 to elicit the production of type-I interferons and cytokines. Recent studies have suggested an auto-inhibitory role for the N-terminal domain (NTD) of TRIF. This domain has no significant sequence similarity to proteins of known structure. In this paper, the crystallization and X-ray diffraction analysis of TRIF-NTD and its selenomethionine-labelled mutant TRIF-NTD$^{A66M/L113M}$ are reported. Thin plate-like crystals of native TRIF-NTD obtained using polyethylene glycol 3350 as precipitant diffracted X-rays to 1.9 Å resolution. To facilitate phase determination, two additional methionines were incorporated into the protein at positions chosen based on the occurrence of methionines in TRIF homologues in different species. Crystals of the selenomethionine-labelled protein were obtained under conditions similar to the wild-type protein; these crystals diffracted X-rays to 2.5 Å resolution. The TRIF-NTD and TRIF-NTD$^{A66M/L113M}$ crystals have the symmetry of space groups $P2_12_12_1$ and $P1$, and most likely contain two and four molecules in the asymmetric unit, respectively. These results provide a sound foundation for the future structure determination of this novel domain.

1. Introduction

Toll-like receptors (TLRs) are pattern-recognition receptors that play key roles in the mammalian innate immune response. The extracellular domain of TLRs binds pathogen-associated molecular patterns (PAMPs), as well as host-derived factors that are indicative of danger (Gay & Gangloff, 2007). This enables oligomerization of TLRs, thus facilitating interactions between the cytoplasmic Toll/interleukin-1 receptor (TIR) domain of the TLRs with specific TIR-domain-containing adaptor proteins (O'Neill & Bowie, 2007). The selective recruitment of one or more specific adaptors to the TLR activates specific downstream signalling cascades, which trigger a broad range of inflammatory and antimicrobial responses (Akira *et al.*, 2006).

Five TIR-domain-containing proteins are usually classified as TLR adaptors in mammals: MyD88 (myeloid differentiation primary response gene 88), MAL (MyD88 adaptor-like protein), TRIF [TIR-domain-containing adaptor inducing interferon (IFN)-β]/TICAM-1 (TIR-domain-containing adaptor molecule 1), TRAM (TRIF-related adaptor molecule) and SARM (sterile α and armadillo motif-containing protein) (Ve *et al.*, 2012). TRIF acts as the sole signalling adaptor for TLR3 and can also associate with TLR4 *via* TRAM, which leads to the production of type-I IFN and cytokines through the activation of transcription factors including IRF3 (IFN regulatory factor 3), NF-κB (nuclear factor-κB) and AP-1 (activator protein-1) (Oshiumi, Matsumoto *et al.*, 2003; Yamamoto *et al.*, 2003; Oshiumi, Sasai *et al.*, 2003; Fitzgerald *et al.*, 2003). Human TRIF consists of 712 amino acids and comprises several domains. The N-terminal region of TRIF contains a TRAF6 (tumour necrosis factor receptor-associated factor 6)-binding motif and interacts with TBK1 (Tank-binding kinase 1), leading to the activation of IRF3 (Sato *et al.*, 2003). The TIR domain is essential for binding to the TIR domain of TLR3 as well as to the adaptor TRAM (Oshiumi, Sasai *et al.*, 2003; Fitzgerald *et al.*, 2003). The C-terminal region contains a receptor-interacting protein (RIP) homotypic interaction motif (RHIM), which recruits

Table 1
Primers used to generate expression constructs.

Primers used for different TRIF constructs (5′ to 3′; labelled corresponding to the relevant N- or C-terminal residue in TRIF)	
Forward: 1	TACTTCCAATCCAATGCCATGGCCTGCACAGGCCCATCACTTCCTAG
Forward: 5	TACTTCCAATCCAATGCCGGCCCATCACTTCCTAGCGCCTTCGAC
Forward: 10	TACTTCCAATCCAATGCCAGCGCCTTCGACATTCTAGGTGCAGCAGG
Reverse: 145	TTATCCACTTCCAATGTTACCCACACCGGTTTCGGGCCTCATCC
Reverse: 150	TTATCCACTTCCAATGTTACCCAGCAATGTCCCACCCACACCGG
Reverse: 153	TTATCCACTTCCAATGTTACCCTGGATCCCCAGCAATGTCCCACC
Reverse: 160	TTATCCACTTCCAATGTTAGGACTGGAGCGTCCGGATGCTCCC
Reverse: 177	TTATCCACTTCCAATGTTAGCTCCTGGTCCCAGAGGGCAAAGCC
Primers used for mutagenesis (5′ to 3′; labelled corresponding to the mutation)	
Forward: A66M	AGAGGCATTGAAGATGGATGCGGTGG
Reverse: A66M	CCACCGCATCCATCTTCAATGCCTCT
Forward: L113M	CCCCGCCTCGATGCGGGACG
Reverse: L113M	CGTCCCGCATCGAGGCGGGG

RIP1 and RIP3, triggering cell death and NF-κB activation (Kaiser & Offermann, 2005).

Recently, it has been reported that the N-terminal region of TRIF comprising residues 1–176 corresponds to a protease-resistant structured domain (Tatematsu *et al.*, 2010). A deletion mutant of TRIF lacking this region (comprising residues 181–712) showed higher NF-κB-dependent IFN-β promoter activation compared with wild-type TRIF, and an interaction between the N-terminal region and the TIR domain was demonstrated by immunoprecipitation and protein fragment complementation analysis. The authors thus proposed that the N-terminal region folds onto the TIR domain of TRIF, preventing self-association until the protein is activated.

Knowledge of the structure of the N-terminal region of TRIF will be of great interest, as it will shed light on the regulation of TRIF and its interaction with the TIR domain. It also promises to reveal a novel structure, as it contains no significant sequence similarity to any proteins of known structure. To this end, we have successfully expressed, purified and crystallized TRIF-NTD (N-terminal domain corresponding to residues 1–153 of TRIF) and its mutant containing two additional Met residues.

2. Materials and methods

2.1. Cloning, protein expression and purification

Fragments encoding residues 1–145, 1–150, 1–153 (TRIF-NTD), 1–160, 1–177, 5–150, 5–153, 10–150 and 10–153 were amplified by PCR from full-length human cDNA and cloned into the pMCSG7 expression vector by ligation-independent cloning (LIC; Stols *et al.*, 2002; for the primers used, see Table 1). The constructs contained an N-terminal hexahistidine (His) tag followed by a TEV (tobacco etch virus) protease cleavage site. The integrity of the constructs was confirmed by sequencing. Subsequently, point mutations were introduced to incorporate additional methionines into the TRIF-NTD protein for selenomethionine labelling, yielding the TRIF-NTD$^{A66M/L113M}$ protein. The mutations were incorporated by conventional PCR in two steps (introducing one mutation first, verifying the integrity of the first mutant construct by sequencing and then introducing the second mutation; for the primers used, see Table 1).

Table 2
Crystallographic data-collection and processing statistics.

Values in parentheses are for the outer shell.

Protein	TRIF-NTD	Se-Met-labelled TRIF-NTD$^{A66M/L113M}$
Diffraction source	MX2, Australian Synchrotron	MX2, Australian Synchrotron
Wavelength (Å)	0.9539	0.9793
Temperature (K)	100	100
Detector	ADSC Quantum 315r CCD	ADSC Quantum 315r CCD
Crystal-to-detector distance (mm)	300.000	399.993
Rotation range per image (°)	0.5	1.0
Total rotation range (°)	360	1440
Exposure time per image (s)	0.5	1.0
Space group	$P2_12_12_1$	$P1$
Unit-cell parameters (Å, °)	a = 48.02, b = 77.18, c = 85.15, $\alpha = \beta = \gamma$ = 90	a = 47.32, b = 49.48, c = 70.32, α = 88.55, β = 77.63, γ = 72.26
Mosaicity (°)	0.34	0.20
Resolution range (Å)	77.18–1.90 (2.01–1.90)	68.62–2.48 (2.63–2.48)
Total No. of reflections	207239	225375
No. of unique reflections	25058	19519
Completeness (%)	99.1 (93.8)	94.8 (68.9)
Anomalous completeness	98.0 (86.7)	93.2 (60.0)
Multiplicity	8.3	11.6
Anomalous multiplicity	4.4	5.8
$\langle I/\sigma(I)\rangle$	6.1 (1.5)	17.1 (4.5)
R_{meas}†	0.206 (1.128)	0.147 (0.614)
$R_{p.i.m.}$‡	0.070 (0.454)	0.043 (0.188)
Overall B factor from Wilson plot (Å^2)	22.5	21.4

† $R_{meas} = \sum_{hkl}\{N(hkl)/[N(hkl)-1]\}^{1/2}\sum_i |I_i(hkl) - \langle I(hkl)\rangle| / \sum_{hkl}\sum_i I_i(hkl)$.
‡ $R_{p.i.m.} = \sum_{hkl}\{1/[N(hkl)-1]\}^{1/2}\sum_i |I_i(hkl) - \langle I(hkl)\rangle| / \sum_{hkl}\sum_i I_i(hkl)$.

The proteins were expressed in *Escherichia coli* BL21 (DE3) cells using auto-induction media (Studier, 2005). The cells were grown by continuous shaking at 230 rev min^{-1} in a temperature-controlled bio-shaker at 310 K in the presence of ampicillin (100 µg l^{-1}). The temperature of the culture was lowered to 293 K when the $OD_{600\ nm}$ reached approximately 0.6–0.8. Subsequently, the cultures were grown for approximately 16 h before harvesting the cells by centrifugation at 5000*g* at 277 K and storing them at 193 K.

For selenomethionine (SeMet) labelling of TRIF-NTD$^{A66M/L113M}$, the construct was expressed in *E. coli* B834 (DE3) (methionine-auxotroph) cells (Novagen) using M9 medium supplemented with 0.2 m*M* SeMet. The cultures were grown at 310 K until the $OD_{600\ nm}$ reached approximately 0.6; at this stage, the temperature of the cultures was lowered to 293 K and IPTG (isopropyl β-D-1-thio-galactopyranoside) was added to the growing medium to a final concentration of 1 m*M* to induce protein expression. The cells were grown approximately 16 h after induction and harvested by centrifugation.

For protein purification, the harvested cells were resuspended in pre-chilled lysis buffer (50 m*M* Tris base pH 8.0, 500 m*M* NaCl, 20 m*M* imidazole, 1 m*M* DTT) at a rate of 5 ml buffer per gram of bacterial cells and lysed using a digital sonifier (Branson). The cell debris and insoluble material were removed by centrifugation at 15 000*g* and 277 K. The resulting supernatant was collected and loaded onto a 5 ml HisTrap FF column (GE Healthcare) which was pre-equilibrated with lysis buffer. To remove unbound proteins and contaminants, the column was washed with 20 column volumes of washing buffer (consisting of 50 m*M* Tris base pH 8.0, 500 m*M* NaCl, 30 m*M* imidazole, 1 m*M* DTT). A linear gradient of 30–500 m*M* imidazole was performed over 20 column volumes to elute the protein and fractions containing TRIF-NTD (as judged by SDS–PAGE) were collected. The collected sample was concentrated to

2 ml using a 10 000 Da molecular-weight cutoff Amicon (Millipore) and then diluted in TEV cleavage buffer (50 m*M* Tris pH 8.0, 250 m*M* NaCl, 1 m*M* DTT, 0.5 m*M* EDTA) to a volume of 20 ml. To remove the N-terminal His tag, 800 µg (at a concentration of 8 mg ml^{-1}) TEV protease was added to 20 ml sample and the tag was removed by overnight digestion. For purification, the digested protein sample was loaded back onto the HisTrap FF column and purified using the same IMAC (immobilized metal-affinity chromatography) strategy as described above. For further purification, the pooled sample was run over the size-exclusion column (Superdex 75 HiLoad 26/60, GE Healthcare) using size-exclusion buffer (20 m*M* HEPES pH 7.5, 150 m*M* NaCl, 2 m*M* DTT). Fractions from the peak were analysed by SDS–PAGE and the purest fractions were pooled together and concentrated. Native protein was concentrated to 56 mg ml^{-1}, whereas the SeMet-labelled protein was concentrated to 20 mg ml^{-1} in size-exclusion buffer. The concentrated proteins were flash-frozen in liquid nitrogen in 50 µl aliquots and stored at 193 K. The concentration of proteins was determined based on the absorbance at 280 nm (NanoDrop ND-1000) using an extinction coefficient of 20 970 M^{-1} cm^{-1}. Multi-angle laser light scattering (MALLS) experiments were carried out using a Dawn Heleos II 18-angle light-scattering detector coupled to an Optilab rEX refractive-index detector (Wyatt Technology) and combined inline with a Superdex 200 10/300 size-exclusion column (GE Healthcare) connected to a Prominence UFLC system (Shimadzu).

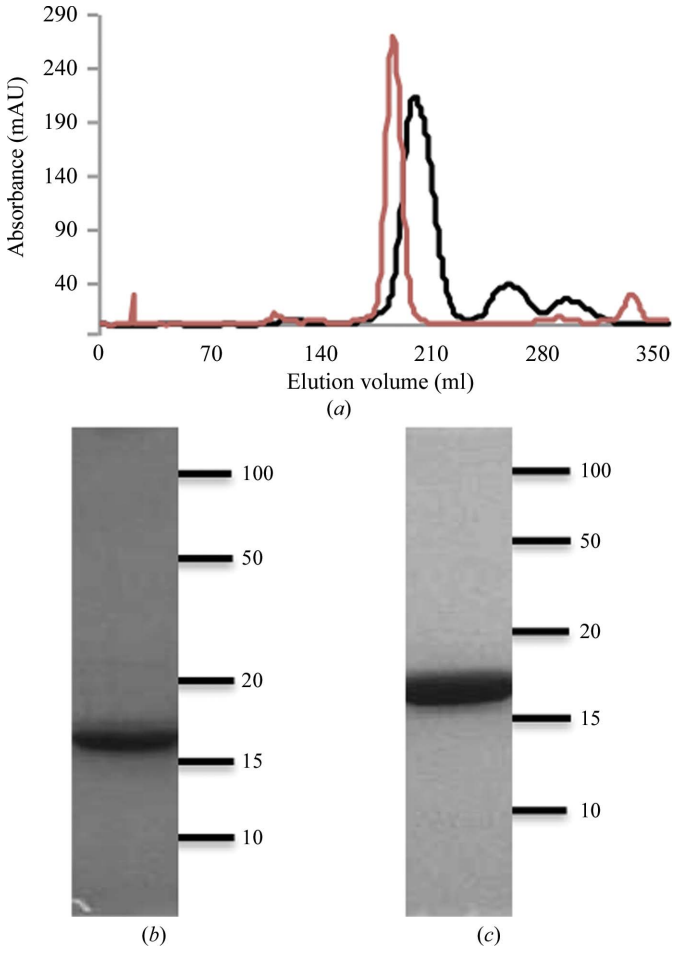

Figure 1
Purification of TRIF-NTD and SeMet-labelled TRIF-NTD$^{A66M/L113M}$. (*a*) Gel-filtration profiles of TRIF-NTD (black) and SeMet-labelled TRIF-NTD$^{A66M/L113M}$ (orange). The two proteins were run using different chromatographic columns. (*b*) SDS–PAGE analysis of purified TRIF-NTD and (*c*) SeMet-labelled TRIF-NTD$^{A66M/L113M}$.

2.2. Crystallization and X-ray data collection

The hanging-drop vapour-diffusion technique was used for crystallization. The optimal protein concentration for crystallization was determined using the PCT screen (Hampton Research). The sparse-matrix approach was used for initial crystallization screening in 96-well plates (LabTech) at 293 K. Several commercial screens [Index, PEG/Ion and PEGRx (Hampton Research), Pact Premier and JCSG+ (Qiagen), Precipitant Synergy (Emerald BioSystems), Systematically Controlled Crystallization Screen Set 101 (Axygen Biosciences) and ProPlex (Molecular Dimensions)] were tested. A total of 1450 crystallization drops were set up for screening using a Mosquito robot (TTP LabTech, UK) on hanging-drop seals (Millennium Science, Australia) by combining 100 nl protein solution and 100 nl reservoir solution and were equilibrated against 75 µl reservoir solution. A Rock Imager system (Formulatrix, USA) was used to monitor the drops.

Crystallization conditions from the initial hits were optimized by varying the concentration of protein and precipitants, the pH and the size of the drop in 24-well or 48-well hanging-drop plates (Hampton Research). For optimization of the crystals, a total of 844 drops were set up for both the native and SeMet-labelled crystals. The cluster of

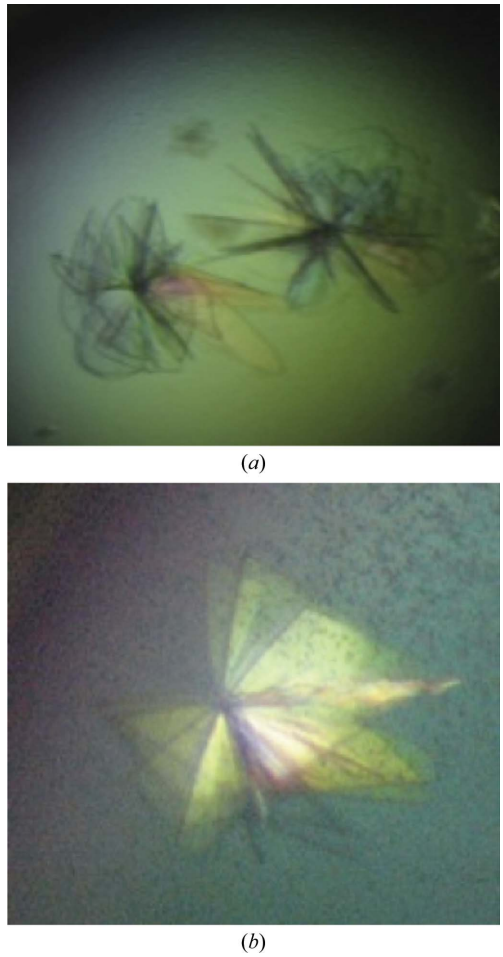

Figure 2
(*a*) Crystals of TRIF-NTD. (*b*) Crystals of SeMet-labelled TRIF-NTD$^{A66M/L113M}$. The crystals measure ∼100 µm in the longest dimension.

crystals was broken into individual plates and individual plate-like crystals were mounted in nylon loops. Prior to flash-cooling in liquid nitrogen, the crystal was transferred to the mother liquor containing 25% glycerol (tests showed that the cryoprotectant was necessary to preserve diffraction).

X-ray diffraction data for both TRIF-NTD and TRIF-NTD$^{A66M/L113M}$ crystals were collected at the Australian Synchrotron (Table 2). In the case of the crystals of SeMet-labelled TRIF-NTD$^{A66M/L113M}$, a fluorescence scan was measured around the selenium absorption edge to identify the absorption peak and the wavelength of 0.9793 Å was chosen based on this.

MOSFLM (Leslie & Powell, 2007) or *XDS* (Kabsch, 2010) were used for indexing and data integration. Data were scaled with *SCALA* (Winn *et al.*, 2011) and analysed by *POINTLESS* (Evans, 2006).

3. Results and discussion

The N-terminal 176 amino acids of TRIF have been previously shown to form a protease-resistant structural domain (Tatematsu *et al.*, 2010). Based on this work, we initially produced a protein corresponding to residues 1–177 of TRIF and subjected it to crystallization. The protein was purified by IMAC and sixe-exclusion chromatography and estimated by SDS–PAGE to be of greater than 95% purity. While sparse-matrix screening of this protein yielded some crystalline material, optimization attempts failed. We therefore prepared a number of shorter constructs, guided by secondary-structure predictions. The best-behaved construct corresponded to residues 1–153 of TRIF (here termed TRIF-NTD). The protein could be purified by IMAC and size-exclusion chromatography to greater than 95% purity, with a yield of 10 mg per litre of bacterial culture. Judging from the gel-filtration profile, the protein was monodisperse, homogeneous and monomeric (Fig. 1). The molecular mass of the native protein was also measured by MALLS and was found to correspond to 15.89 ± 2.38 kDa (the theoretical mass corresponds to 16.99 kDa), consistent with a monomeric protein.

Crystallization screens for native TRIF-NTD yielded clusters of needle-like microcrystals under 15 different conditions after 2–3 d, most with conditions containing PEGs of different molecular weights as precipitant. Based on the morphology of the crystals, we chose Index screen condition No. 79 (0.1 *M* bis-tris pH 6.5, 200 m*M* NaCl, 25% PEG 3350) for further optimization. To grow single crystals of larger size, we varied the pH, the presence of salts and their concentration, alternative precipitants and their concentration, different protein:reservoir solution ratios in the drop and drop volume and different additives. Thin plate-like crystals suitable for data collection were obtained in 0.1 *M* bis-tris pH 6.6, 150 m*M* NaCl, 21% PEG 3350 using a protein concentration of 30 mg ml^{-1} (Fig. 2). Flash-cooled crystals diffracted X-rays to 1.9 Å resolution.

TRIF-NTD shares no significant sequence similarity with any proteins of known structure and therefore structure determination will require experimental phasing. The crystallized protein contains two methionines, one of which is the N-terminal residue. We reasoned that it would be beneficial to introduce additional Met residues. We analysed a multiple sequence alignment of TRIF homologues and found two positions, corresponding to Ala66 and Leu113 in human TRIF, where Met occurred in some of the homologues (Fig. 3). We used site-directed mutagenesis to generate the TRIF-NTD$^{A66M/L113M}$ construct. We were able to successfully express and purify SeMet-labelled TRIF-NTD$^{A66M/L113M}$ (with a yield of 15 mg per litre of bacterial culture; Fig. 1) and crystallize it under conditions similar to native TRIF-NTD (0.1 *M* bis-tris pH 6.6, 150 m*M* NaCl, 28% PEG 3350; protein concentration 20 mg ml^{-1}; Fig. 2). The crystals had a morphology similar to the crystals of the native protein and diffracted X-rays to 2.5 Å resolution.

The crystals of native TRIF-NTD have the symmetry of space group $P2_12_12_1$, while the SeMet-labelled crystals of TRIF-NTD$^{A66M/L113M}$ have the symmetry of space group $P1$ (Table 2). The former and the latter are most likely to contain two and four molecules in the asymmetric unit, respectively (corresponding to a Matthews coefficient of 2.38 Å^3 Da^{-1}, a solvent content of 48.3% and a probability of 0.68 for TRIF-NTD and a Matthews coefficient of

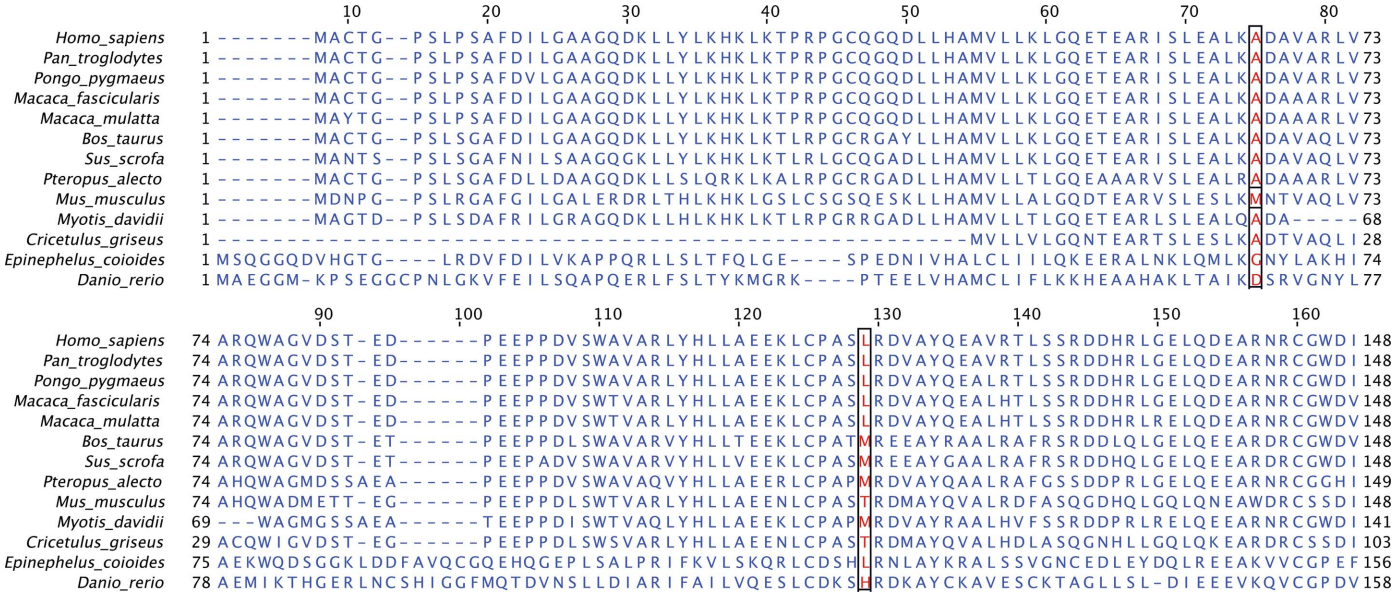

Figure 3
Multiple sequence alignment of the N-terminal region of TRIF from different species. Red-coloured columns highlight the positions corresponding to Ala66 and Leu113 in human TRIF, where methionine substitutions can be found in other species.

2.32 Å^3 Da^{-1}, a solvent content of 47% and a probability of 97% for TRIF-NTD$^{A66M/L113M}$; analysed using the *Matthews Probability Calculator*; Matthews, 1968; Kantardjieff & Rupp, 2003).

The described crystals form a sound foundation to determine the structure of TRIF-NTD by SAD (single-wavelength anomalous diffraction) phasing and this work is currently under way. Because the crystallized domain of TRIF contains no significant sequence similarity to any proteins of known structure, it may reveal a novel protein fold. The structure will also shed light on the regulation of TRIF and the interaction of TRIF-NTD with the TIR domain.

We thank Eugene Valkov, Simon Williams, Rafael Counago and other members of the Kobe laboratory for help and discussions. This work was supported by the National Health and Medical Research Council (NHMRC grant 1003326 to BK and AM). BK is an NHMRC Research Fellow. MJS is the recipient of an Australian Research Council Future Fellowship (FT100100657), as well as an Honorary NHMRC Senior Research Fellowship (APP1003470).

References

Akira, S., Uematsu, S. & Takeuchi, O. (2006). *Cell*, **124**, 783–801.
Evans, P. (2006). *Acta Cryst.* D**62**, 72–82.
Fitzgerald, K. A., Rowe, D. C., Barnes, B. J., Caffrey, D. R., Visintin, A., Latz, E., Monks, B., Pitha, P. M. & Golenbock, D. T. (2003). *J. Exp. Med.* **198**, 1043–1055.
Gay, N. J. & Gangloff, M. (2007). *Annu. Rev. Biochem.* **76**, 141–165.
Kabsch, W. (2010). *Acta Cryst.* D**66**, 125–132.
Kaiser, W. J. & Offermann, M. K. (2005). *J. Immunol.* **174**, 4942–4952.
Kantardjieff, K. A. & Rupp, B. (2003). *Protein Sci.* **12**, 1865–1871.
Leslie, A. G. W. & Powell, H. R. (2007). *Evolving Methods for Macromolecular Crystallography*, edited by R. Read & J. L. Sussman, pp. 41–51. Dordrecht: Springer.
Matthews, B. W. (1968). *J. Mol. Biol.* **33**, 491–497.
O'Neill, L. A. & Bowie, A. G. (2007). *Nature Rev. Immunol.* **7**, 353–364.
Oshiumi, H., Matsumoto, M., Funami, K., Akazawa, T. & Seya, T. (2003). *Nature Immunol.* **4**, 161–167.
Oshiumi, H., Sasai, M., Shida, K., Fujita, T., Matsumoto, M. & Seya, T. (2003). *J. Biol. Chem.* **278**, 49751–49762.
Sato, S., Sugiyama, M., Yamamoto, M., Watanabe, Y., Kawai, T., Takeda, K. & Akira, S. (2003). *J. Immunol.* **171**, 4304–4310.
Stols, L., Gu, M., Dieckman, L., Raffen, R., Collart, F. R. & Donnelly, M. I. (2002). *Protein Expr. Purif.* **25**, 8–15.
Studier, F. W. (2005). *Protein Expr. Purif.* **41**, 207–234.
Tatematsu, M., Ishii, A., Oshiumi, H., Horiuchi, M., Inagaki, F., Seya, T. & Matsumoto, M. (2010). *J. Biol. Chem.* **285**, 20128–20136.
Ve, T., Gay, N. J., Mansell, A., Kobe, B. & Kellie, S. (2012). *Curr. Drug Targets*, **13**, 1360–1374.
Winn, M. D. *et al.* (2011). *Acta Cryst.* D**67**, 235–242.
Yamamoto, M., Sato, S., Hemmi, H., Hoshino, K., Kaisho, T., Sanjo, H., Takeuchi, O., Sugiyama, M., Okabe, M., Takeda, K. & Akira, S. (2003). *Science*, **301**, 640–643.